Please verify that (1) all pages are present, (2) all figures are correct, (3) all fonts and special characters are correct, and (4) all text and figures fit within the red margin lines shown on this review document. Complete formatting information is available at http://SPIE.org/manuscripts

Return to the Manage Active Submissions page at http://spie.org/app/submissions/tasks.aspx and approve or disapprove this submission. Your manuscript will not be published without this approval. Please contact author_help@spie.org with any questions or concerns.

Thin-film, wide-angle, design-tunable, selective absorber from near UV to far infrared

Janardan Nath[a], Douglas Maukonen[a], Evan Smith[a], Pedro Figueiredo[a], Guy Zummo[a], Deep Panjwani[a], Robert E. Peale[a], Glenn Boreman[b], Justin W. Cleary[c], Kurt Eyink[d]

[a]Department of Physics, University of Central Florida, Orlando FL 32816

[b]Department of Physics and Optical Science, University of North Carolina at Charlotte, Charlotte, NC 28223

[c]Air Force Research Laboratory, Sensors Directorate, Wright Patterson AFB OH 45433

[d]Air Force Research Laboratory, Materials and Manufacturing Directorate, Wright Patterson AFB OH 45433

ABSTRACT

We experimentally demonstrate a structured thin film that selectively absorbs incident electromagnetic waves in discrete bands, which by design occur in any chosen range from near UV to far infrared. The structure consists of conducting islands separated from a conducting plane by a dielectric layer. By changing dimensions and materials, we have achieved broad absorption resonances centered at 0.36, 1.1, 14, and 53 microns wavelength. Angle-dependent specular reflectivity spectra are measured using UV-visible or Fourier spectrometers. The peak absorption ranges from 85 to 98%. The absorption resonances are explained using the model of an LCR resonant circuit created by coupling between dipolar plasma resonance in the surface structures and their image dipoles in the ground plane. The resonance wavelength is proportional to the dielectric permittivity and to the linear dimension of the surface structures. These absorbers have application to thermal detectors of electromagnetic radiation.

Keywords: Selective absorbers, metamaterial absorber, plasmonics, near-IR, Long wave infra-red (LWIR), far-IR.

1. INTRODUCTION

Wavelength-selective absorbers have a wide range of applications including microbolometers [1], thermal imaging [2, 3], coherent thermal emitters [4], solar cells [5], thermal photovoltaic solar energy conversion [6,7] and refractive index sensing [8,9]. Resonant plasmonic and metamaterial structures are being investigated widely and are reported to produce perfect absorption up to 99% in the visible [10], near- and mid- infrared [11, 12], and terahertz frequencies[13]. The resonance frequency depends on the size of the structures[14]. The resonant absorption typically has bandwidth less than 12% of the center frequency[14]. Both experimental and numerical studies suggest that 99.99% absorption can be achieved with these kinds of absorbers in any frequency range, from optical to terahertz [3, 4, 10, 13]. The resonance absorption occurs by excitation of localized magnetic and electric dipoles[10, 13]. Structures may be designed to be polarization independent and omnidirectional[12 - 15]. These absorbers have been studied both by simulations and experiments. Analytic theory has been less extensively applied, though it promises simple design rules and an understanding of underlying physics. In this paper we study these absorbers experimentally and interpret the spectra in terms of a simple analytic model. Fabrication is by standard photolithography and is compatible with MEMS processing. Silicon dioxide is the chosen dielectric for compatibility with such processing, although silicon dioxide has strong absorption and dispersion near 10 micron wavelengths.

2. THEORITICAL CONSIDERATIONS

Figure 1(a) presents a schematic of the considered structure. Surface conductors are taken to be squares arranged in a checkerboard pattern. The squares are situated on top of a dielectric layer, which itself is supported by a metal ground plane. Gold is taken as the conductor material and silicon dioxide as the dielectric spacer. Simulations [12, 13, 16] demonstrate excitation of fundamental and higher order resonances and corresponding absorption of the driving fields. In the case of the fundamental, the incident electric field excites an electric dipole in the gold square. An image dipole is excited in the gold film under the spacer material. The driven current sloshing back and forth between the ends of the

SPIE USE: ____ DB Check, ____ Prod Check, Notes:

Please verify that (1) all pages are present, (2) all figures are correct, (3) all fonts and special characters are correct, and (4) all text and figures fit within the red margin lines shown on this review document. Complete formatting information is available at http://SPIE.org/manuscripts

Return to the Manage Active Submissions page at http://spie.org/app/submissions/tasks.aspx and approve or disapprove this submission. Your manuscript will not be published without this approval. Please contact author_help@spie.org with any questions or concerns.

square, with opposite polarity in the ground plane, can be considered as charging and discharging capacitors located at the ends of the square. The resonant frequency is given by[13]

$$f = \frac{\sqrt{2}}{2\pi\sqrt{LC}} \tag{1}$$

where L is the mutual parallel plate inductance and C is the capacitance, which depend on the thickness of dielectric t and size of the absorber l, permeability, and dielectric permittivity according to $L = \mu_0\mu_r t$ and $C = \varepsilon_0\varepsilon_r l^2/2t$. For all media used in our work, the relative permeability has the value unity. The permittivity of SiO_2 is complex in the infrared due to absorption and dispersion. From Eq. (1) and the expressions for L and C, we find the fundamental resonance wavelength to be

$$\lambda = \pi l\, n(\lambda) \tag{2}$$

where $n(\lambda)$ is the refractive index of the spacer material.

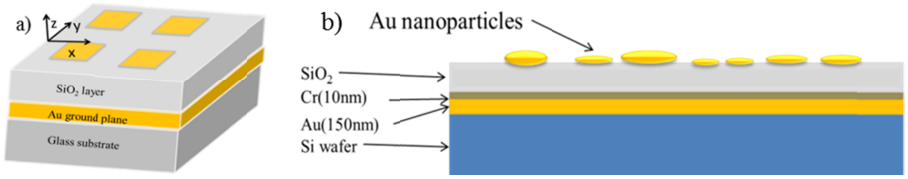

Figure 1. (a) Schematic diagram of selective infrared absorber. (b) Absorbers in UV and NIR formed by gold nano-islands.

For our deposited SiO_2 layers in the wavelength range 5-20 microns, we obtained the refractive index n and absorption coefficient k experimentally using a VASE IR ellipsometer for a 1.4 micron layer of electron beam evaporated SiO_2 on top of 10 nm Cr on 150 nm of gold . These data are presented in Fig. 2. Values for the UV-Visible and far infra-red regions are taken from references [17] and [18].

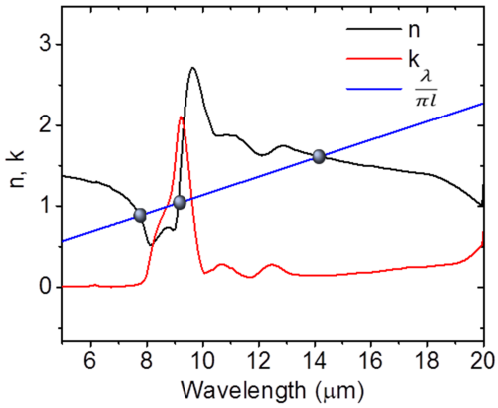

Figure 2. Black and red curves represent experimentally measured refractive index n and absorption coefficient k respectively as a function of wavelength for SiO_2. The blue line is a plot of $\lambda/\pi l$, where l =2.8μm. Intersections give resonance solutions as 14.26, 9.07, and 7.73 μm.

Resonant wavelengths are found by solving equation (2), which is easily done graphically. Figure 2 presents plots of $n(\lambda)$ and $\lambda/\pi l$ for one of the samples fabricated without the final array of gold squares. Resonances occur at the points of intersection. For this sample, 3 resonances are found, which we denote by λ_i, where i= 1, 2, 3. These are 14.26, 9.07, and 7.73 μm, respectively. In the UV, visible or far infra-red region where dispersion is slight, equation 2 is simply solved to give single resonance wavelengths.

Please verify that (1) all pages are present, (2) all figures are correct, (3) all fonts and special characters are correct, and (4) all text and figures fit within the red margin lines shown on this review document. Complete formatting information is available at http://SPIE.org/manuscripts

Return to the Manage Active Submissions page at http://spie.org/app/submissions/tasks.aspx and approve or disapprove this submission. Your manuscript will not be published without this approval. Please contact author_help@spie.org with any questions or concerns.

3. EXPERIMENTS AND RESULTS

We fabricated absorbers by two methods depending on the wavelength region. For the mid- to far-IR region, gold squares were patterned by photolithography and conventional metal lift-off (Fig. 1.a). A 150 nm thick layer of gold was deposited by electron beam evaporation on a glass or Si substrate. Then, SiO_2 was deposited as a dielectric spacer by either plasma enhanced chemical vapor deposition or by electron beam evaporation. Square patterns of gold as shown in figure 3 were fabricated on the SiO_2 film by standard photolithography, e-beam evaporation, and lift-off. For the sample with evaporated SiO_2, a 10 nm layer of Cr was also deposited before deposition of SiO_2 as a sticking layer. Dimension of the squares and their period were determined by confocal microscopy. Samples were similarly prepared without the surface squares for comparison.

Table 1. Absorber parameters

Active region	SiO_2 thickness, t	Absorber size, l	Predicted absorption
Near-UV(0.3-0.4μm)	30nm	71.5nm	348nm
Near IR (1-3μm)	180nm	282.3nm	1241nm
Long-wave-IR (8-20μm)	1.4μm	2.8μm	14.26, 9.07, 7.73μm
Far-IR(30-80μm)	2.2μm	10μm	62.3μm

For the near-UV to near-IR region, randomly distributed gold nano-islands were formed by annealing thin gold films (Fig. 1.b). We sequentially deposited by electron beam evaporation on a Si wafer a 10 nm Cr sticking layer, 150 nm of gold, a 10 nm Cr sticking layer, and SiO_2. Then, an optically thin film of gold was deposited by DC sputtering. This optically thin and discontinuous gold film becomes irregularly shaped islands of gold nano-discs on annealing at 300 C for 90 minutes. Particle size-distributions were determined using ImageJ[19]. Table 1 represents dielectric layer thickness and absorber size for different samples.

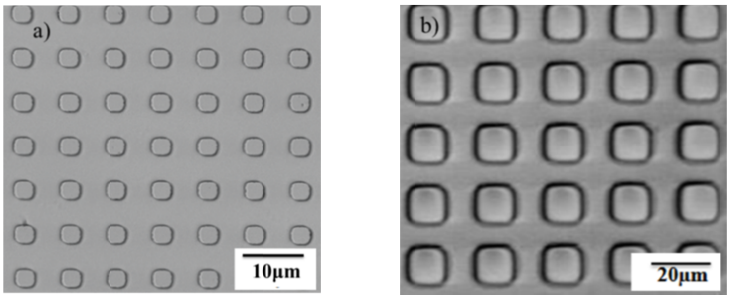

Figure 3. Confocal microscope image of the sample surface (a) with 2.8 μm size squares and periodicity 7.5 μm and (b) with 10 μm size squares and periodicity 20 μm.

LWIR Reflectivity was measured using a PerkinElmer Spectrum One FTIR spectrometer with microscope accessory in reflectivity mode with angles of incidence spanning 19 to 31 degrees. Far-IR reflectivity was measured by a BOMEM DA8 spectrometer at near normal incidence with 6 micron Mylar beam splitter. UV-Vis-NIR reflectivity was measured using a Cary 500i spectrometer with a variable angle specular reflectivity accessory (VARSA) covering angles of incidence from 20 to 50 deg. The reflectivity for these structures is supposed to be fairly independent of incidence angle[12, 13, 15]. Reflectance R is obtained by dividing the raw reflected power spectrum with that of an optically thick smooth gold film. Transmittance through the sample is zero because the gold film at the bottom is optically thick. Thus, absorptance A can be found from $A = 1 - R$, assuming scattering to be negligible because the particle size is much smaller than the wavelength of incident light.

3.1 LW-IR and far-IR absorbers

Reflectance spectra for far IR and LWIR samples, with and without gold squares on the top surface, are presented in Figure 4. The samples without squares on their surface (black curves) have the highest reflectivity baseline. For the LWIR sample, the absorption that appears when the squares are present overlaps the native absorption bands of the oxide

Please verify that (1) all pages are present, (2) all figures are correct, (3) all fonts and special characters are correct, and (4) all text and figures fit within the red margin lines shown on this review document. Complete formatting information is available at http://SPIE.org/manuscripts

Return to the Manage Active Submissions page at http://spie.org/app/submissions/tasks.aspx and approve or disapprove this submission. Your manuscript will not be published without this approval. Please contact author_help@spie.org with any questions or concerns.

dielectric, which occur as a sharp peak at 6.2 microns, a partially resolved doublet at 8 and 8.7 microns, a stronger partially resolved doublet at 9.7 and 10.7 microns, and a clear band at 12.5 microns. Significantly, the oxide reference sample lacks any significant absorption bands in the wavelength range 12-20 microns.

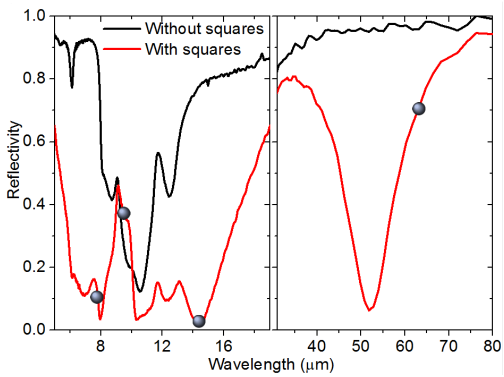

Figure 4. LWIR (left) and far-IR (right) reflectance spectra. Black lines are spectra from samples without squares. Black dots represent theoretically calculated resonances. The peak LWIR and far-IR absorptances are 98% and 95%, respectively.

When the squares are added to the surface of the LWIR sample, the spectrum changes significantly. A new strong band appears at 7 microns. The unresolved bands 8 and 8.7 microns both deepen, but their relative strength changes dramatically. The band at 9.7 microns actually gets weaker, while its partner at 10.7 microns becomes much stronger with a shoulder appearing at 11.2 microns. Most significantly, a very strong and broad band appears at 14.3 microns, where there was no absorption before. Symbols indicate the wavelength positions of the three fundamental resonances determined graphically in Fig. 2. There is fair agreement for the predicted resonances λ_1 =14.26 and λ_3=7.73 microns and the observed bands at 14.3 and 8 microns, The predicted λ_2=9.07 micron band does not account for the reduced absorption at 9.7 microns, unless for some reason this resonance has actually blue shifted in contrast to the other two. The weakening of absorption strength at 9.7 micron due to the reduction in the absorption by SiO_2 is caused by shadowing from the gold squares. None of the predicted resonances corresponds to the broad band at 6.9 microns, but we note that this wavelength is about half that of the observed band at 14.3 micron and may be a harmonic.

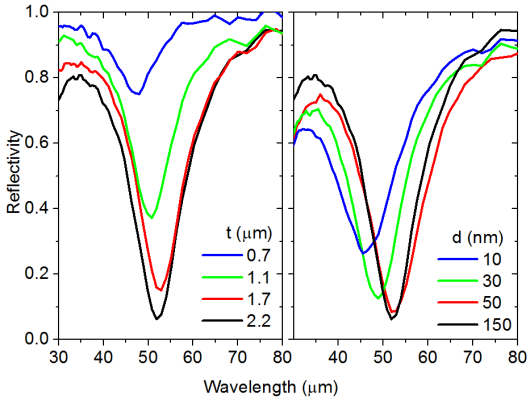

Figure 5. Reflectivity spectra for several far-IR samples for (left) different dielectric thicknesses at constant gold thickness, and (left) different gold square thicknesses at constant dielectric thickness.

In Figure 4 (right), the reflectivity spectrum for the far-IR sample without squares confirms the absence of significant absorption for SiO_2 in the wavelength range 30-80 microns. When squares are added, a strong band with 95% peak absorption appears centered at 53 microns wavelength. According to Eq. 2, the resonance should appear at λ =62 micron wavelength using n = 2 for SiO_2[18]. Ref [18] reported indices of SiO_2 from different papers, and it varies in the range of 1.96 to 2.10 in 50-60 micron range. It is reported that the refractive index and absorption index varies with deposition

Please verify that (1) all pages are present, (2) all figures are correct, (3) all fonts and special characters are correct, and (4) all text and figures fit within the red margin lines shown on this review document. Complete formatting information is available at http://SPIE.org/manuscripts

Return to the Manage Active Submissions page at http://spie.org/app/submissions/tasks.aspx and approve or disapprove this submission. Your manuscript will not be published without this approval. Please contact author_help@spie.org with any questions or concerns.

methods and parameters[18]. The mismatch of predicted resonance with the experimental value may be due, all or in part, to the uncertainty in n.

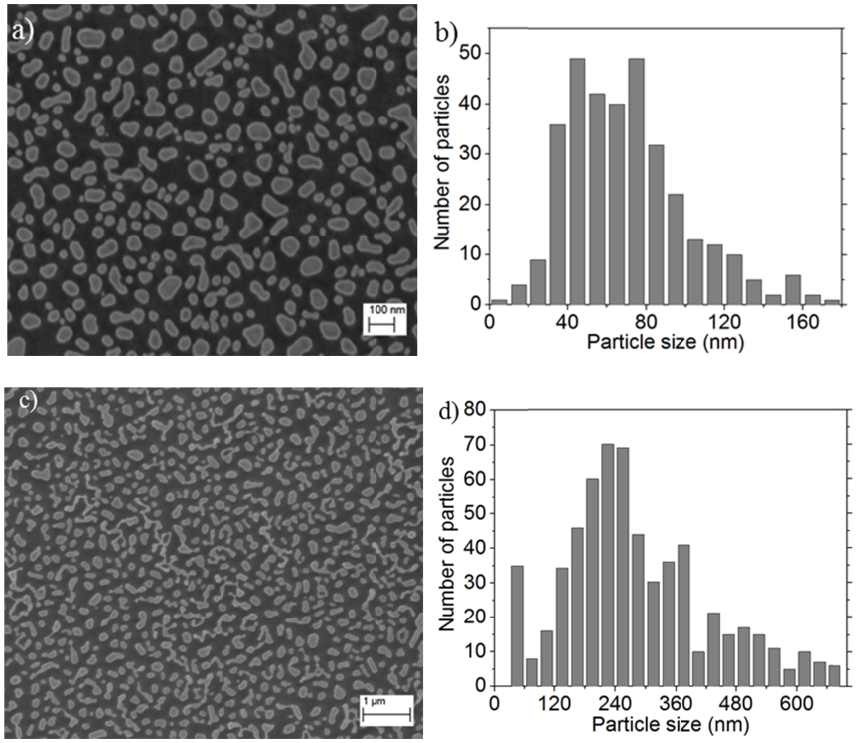

Figure 6. Scanning microscope images of gold nano-islands on oxide for two different initial thickness of sputtered gold film. Particle size distributions are plotted adjacent to each image.

Figure 5 (left) presents reflectivity spectra for several far-IR samples having different dielectric thicknesses but with the same 150 nm thickness of the gold squares. As the dielectric thickens from 0.7 to 2.2 microns, the peak absorption increases from 20 to 95% and the resonance wavelength red shifts by ~10%. Calculation of the equivalent circuit inductance considers only the magnetic energy in the space between the conductors and not within them. As this space is reduced and begins to become comparable to the thickness of the conductors, the relative contribution of the magnetic energy inside the conductors should become more important, and one would expect the resonance response to change.

Figure 5(right) presents reflectance spectra for several far-IR samples having the same 2.2 micron SiO_2 thickness but different thicknesses of the gold squares. As the gold squares thicken from 10 to 150 nm, the peak absorption increases from 52% to 95% and the resonance wavelength red shifts by ~15%. The 50 and 150 nm thick gold squares (red and black lines in figure 5(right) are both thicker than the skin-depth and therefore have the same IR resistivity[20], so it is unsurprising that their optical response is the same. Thicknesses of 30 nm and below are less than the skin-depth, so that the electrical properties of the circuit must change, so it is not surprising that the resonance response and depth would be different.

3.2 Near-UV to near-IR absorbers

Figure 6 presents an SEM image of the gold nano-islands formed by annealing optically thin gold films. The bar graphs in figure 6(right) represent the island size distribution. The peak of the distribution depends on the initial thickness of the gold film before annealing to form islands. When the thickness of Au film is 10 nm, the average particle size is 71.5 nm, giving a sample that absorbs in the near UV. When the film thickness was 30 nm, the average particle size is 282.3 nm, giving a sample that absorbers in the near IR.

Please verify that (1) all pages are present, (2) all figures are correct, (3) all fonts and special characters are correct, and (4) all text and figures fit within the red margin lines shown on this review document. Complete formatting information is available at http://SPIE.org/manuscripts

Return to the Manage Active Submissions page at http://spie.org/app/submissions/tasks.aspx and approve or disapprove this submission. Your manuscript will not be published without this approval. Please contact author_help@spie.org with any questions or concerns.

Figure 7(left) presents reflectivity spectra for the near-UV and near-IR samples. For the near UV sample, absorption peaks at 95% for 360 nm wavelength. The absorption band width relative to the resonance center wavelength is nearly unity for both samples, while the relative widths at LWIR and far-IR wavelengths were about 20%. The difference is understandable in terms of the gold-island size distributions compared with the mono-disperse squares. From the average island size the resonance wavelengths from equation 2, are λ =348 nm and 1.249 μm, in good agreement with the observed values of 360 nm and 1.134μm.

Reflectivity spectra of samples without gold nano-islands are represented by thinner lines in figure 7, and both samples reveal the known SiO_2 absorption band at ~296 nm [21]. Figure 7 (right) present reflectivity spectra for near-UV and near-IR samples for different angles of incidence from 20 to 50 degrees. Strong absorption is sustained to wide angle of incidence and the absorption blue shifts somewhat as this angle is increased.

4. SUMMARY AND CONCLUSION

We have experimentally demonstrated strong design-tunable absorption bands in the near-UV, near-, mid-, and far-IR wavelength regions for a surface composed of gold squares or islands separated from a gold plane by a SiO_2 dielectric layer. The positions of the resonances are predicted with reasonable accuracy using a simple analytic model. Optimum thickness of the dielectric is required for the perfect absorption to occur. This absorption is sustained to wide angle of incidence up to 50 degrees. More than ~80% of absorption is achieved in the range of 6-16 microns which includes the LWIR atmospheric transmission window. This can be useful for thermal detectors working in this range.

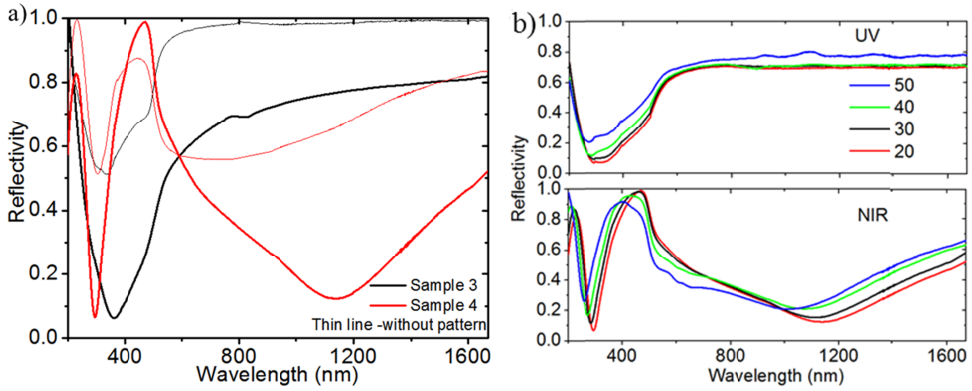

Figure 7. (a) Reflectivity spectra in near-UV and near-IR. Thick lines represent reflectivity spectra from samples with gold nano-islands, while thinner lines represent spectra from samples without the gold nano-islands. (b) Reflectivity spectra with varying angle of incidence, as indicated in deg in the legend.

ACKNOWLEDGEMENTS

This work was supported in part by a grant from the Florida High Technology Corridor (I-4) program. Travel funds for attending this meeting were provided by the UCF Student Government Association and the UCF Division of Graduate Studies.

REFERENCES

[1] Mauskopf, P. D., Bock, J. J., Del Castillo, H., Holzapfel, W. L. and Lange, A. E., "Composite infrared bolometers with Si_3N4 micromesh absorbers," Appl. Opt. 36, 765–771 (1997).
[2] Parsons, A. D. and Pedder, D. J., "Thin-film infrared absorber structures for advanced thermal detectors," J. Vac. Sci. Technol. A 6, 1686–1689 (1988).
[3] Liu, X., Starr, T., Starr, A. F. and Padilla, W. J., "Infrared Spatial and Frequency Selective Metamaterial with Near-Unity Absorbance," Phys. Rev. Lett. 104, 1-4, (2010).

Please verify that (1) all pages are present, (2) all figures are correct, (3) all fonts and special characters are correct, and (4) all text and figures fit within the red margin lines shown on this review document. Complete formatting information is available at http://SPIE.org/manuscripts

Return to the Manage Active Submissions page at http://spie.org/app/submissions/tasks.aspx and approve or disapprove this submission. Your manuscript will not be published without this approval. Please contact author_help@spie.org with any questions or concerns.

[4] Diem, M., Koschny, T. and Soukoulis, C., "Wide-angle perfect absorber/thermal emitter in the terahertz regime," Phys. Rev. B79, 1-4, (2009).
[5] Pillai, S., Catchpole, K. R., Trupke, T., and Green, M. A., "Surface plasmon enhanced silicon solar cells," J. Appl. Phys. 101, 093105 (2007).
[6] Rephaeli, E. and Fan, S., "Absorber and emitter for solar thermo-photovoltaic systems to achieve efficiency exceeding the Shockley-Queisser limit," Optics Express 17, 15145-15159 (2009).
[7] Rand, B. P., Peumans, P. and Forrest, S. R., "Long-range absorption enhancement in organic tandem thin-film solar cells containing silver nanoclusters," J. Appl. Phys. 96, 7519–7526 (2004).
[8] Liu, N., Mesch, M., Weiss, T., Hentschel, M. and H. Giessen, "Infrared perfect absorber and its application as plasmonic sensor," Nano Lett. 10, 2342-23428 (2010).
[9] Wang, Xiaonong, Luo, Chunrong, Hong, Gang and Zhao, Xiaopeng, "Metamaterial optical refractive index sensor detected by the naked eye", Appl. Phys. Lett. 102, 091902 (2013).
[10] Hedayati, M. K., Javaherirahim, M., Mozooni, B., Abdelaziz, R., Tavassolizadeh, A., Chakravadhanula, V. S. K., Zaporojtchenko, V., Strunkus, T., Faupe, F. and Elbahri, M., "Design of a perfect black absorber at visible frequencies using plasmonic metamaterials," Advanced Materials 23, 5410-5414 (2011).
[11] Wang, J., Chen, Y., Hao, J., Yan, M. and Qiu, M., "Shape-dependent absorption characteristics of three-layered metamaterial absorbers at near-infrared," J. Appl. Phys. 109, 074510 (2011).
[12] Hendrickson, J., Guo, J., Zhang, B., Buchwald, W. and Soref, R., "Wideband perfect light absorber at midwave infrared using multiplexed metal structures," Optics Lett. 37, 371-373 (2012).
[13] Ye, Y. and Jin, Y., "Omnidirectional, polarization-insensitive and broadband thin absorber in the terahertz regime," JOSA B 27, 498-504 (2010).
[14] Hao, J., Wang, J., Liu, X., Padilla, W. J., Zhou, L., and Qiu, M., "High performance optical absorber based on a plasmonic metamaterial," Appl. Phys. Lett. 96, 251104 (2010).
[15] Alici, K. B., Turhan, A. B., Soukoulis, C. M. and Ozbay, E., "Optically thin composite resonant absorber at the near-infrared band: a polarization independent and spectrally broadband configuration," Optics Express 19, 14260-7 (2011).
[16] Hao, J., Zhou, L. and Qiu, M., "Nearly total absorption of light and heat generation by plasmonic metamaterials", Physical Review B 83, 1–12 (2011).
[17] Palik, E. D., [Handbook of Optical Constants of Solids], Academic Press, 1985.
[18] Kitamura, R., Pilon, L. and Jonasz, M., "Optical constants of silica glass from extreme ultraviolet to far infrared at near room temperature," Appl. Optics 46, 8118-8133 (2007).
[19] Collins, T. J., "ImageJ for microscopy," BioTechniques 43 (1 Suppl): 25–30 (July 2007).
[20] Bourque-Viens, A., Aimez, V., Taberner, A., Poul, Nielsen, Charette, P. G., "Modelling and experimental validation of thin-film effects in thermopile-based microscale calorimeters", Sensors and Actuators A: Physical 150, 199–206 (2009).
[21] Khashan, M. and Nassif, A., "Dispersion of the optical constants of quartz and polymethyl methacrylate glasses in a wide spectral range: 0.2–3 m," Opt. Commun. 188, 129–139 (2001).